AD-A274 325

(2)

Semiannual Technical Report

Atomic Layer Epitaxy of Group IV Materials: Surface Processes, Thin Films, Devices and Their Characterization

DTIC
ELECTE
DEC 30 1993
S A

Supported under Grant #N00014-91-J-1416
Office of the Chief of Naval Research
Report for the period 7/1/93-12/31/93

R. F. Davis, S. Bedair*, N. A. El-Masry and J. T. Glass
T. Chikyow*, P. Goeller, S. King, J. Sumakeris,
D. Tucker and L. Tye
c/o Materials Science and Engineering Department
and *Electrical and Computer Engineering Department
North Carolina State University
Campus Box 7907
Raleigh, NC 27695-7907

This document has been approved for public release and sale; its distribution is unlimited.

December, 1993

93-31395

93 12 27 127

REPORT DOCUMENTATION PAGE

Form Approved
OMB No. 0704-0188

Public reporting burden for this collection of information is estimated to average 1 hour per response, including the time for reviewing instructions, searching existing data sources, gathering and maintaining the data needed, and completing and reviewing the collection of information. Send comments regarding this burden estimate or any other aspect of this collection of information, including suggestions for reducing this burden to Washington Headquarters Services, Directorate for Information Operations and Reports, 1215 Jefferson Davis Highway, Suite 1204, Arlington, VA 22202-4302, and to the Office of Management and Budget Paperwork Reduction Project (0704-0188), Washington, DC 20503.

1. AGENCY USE ONLY *(Leave blank)*

2. REPORT DATE
December, 1993

3. REPORT TYPE AND DATES COVERED
Semiannual Technical 7/1/93–12/31/93

4. TITLE AND SUBTITLE
Atomic Layer Epitaxy of Group IV Materials: Surface Processes, Thin Films, Devices and Their Characterization

5. FUNDING NUMBERS
414v001---01
1114SS
N00179
N66005
4B855

6. AUTHOR(S)
Robert F. Davis, Salah Bedair, Nadia El-Masry and Jeffrey T. Glass

7. PERFORMING ORGANIZATION NAME(S) AND ADDRESS(ES)
North Carolina State University
Hillsborough Street
Raleigh, NC 27695

8. PERFORMING ORGANIZATION REPORT NUMBER
N00014-91-J-1416

9. SPONSORING/MONITORING AGENCY NAMES(S) AND ADDRESS(ES)
Sponsoring: ONR, Code 314, 800 N. Quincy, Arlington, VA 22217-5660
Monitoring: Office of Naval Research Resider
The Ohio State University Research Center
1960 Kenny Road
Columbus, OH 43210-1063

10. SPONSORING/MONITORING AGENCY REPORT NUMBER

11. SUPPLEMENTARY NOTES

12a. DISTRIBUTION/AVAILABILITY STATEMENT
Approved for Public Release; Distribution Unlimited

12b. DISTRIBUTION CODE

13. ABSTRACT *(Maximum 200 words)*

Atomic layer epitaxy of monocrystalline β-SiC on Si(100) and α(6H)-SiC(0001) substrates has been accomplished at 850°C by alternating the supplies of Si_2H_6, C_2H_4 and atomic hydrogen and without the use of a carbonizing step. Conformal deposition of SiC has been demonstrated within trenches etched into Si(100) wafers. P-type films have also been achieved using Al as a dopant. Devices including HBTs with β-SiC emitters have been designed. Hydrogen plasma cleaning of SiC surfaces has been studied. XPS has shown that this process effectively removes C-O, C-F and C-H bonding at the surface. Temperature programmed desorption has been used to look at the amount of subsurface hydrogen generated during plasma cleaning. The diamond precursors of chlorinated methylsilanes and the substrate of Si(100) were subjected to bias enhanced high-frequency CVD. No difference in diamond nucleation density between the precursors was observed. An interface structure of single crystal CeO_2/Si(111) grown by laser ablation has been investigated. An interfacial reaction occurred between these phases during deposition which resulted in the formation of an oxygen deficient amorphous(a) CeO_x layer and an SiO_2 layer. Post annealing in O_2 caused the disappearance of the a-CeO_x and the regrowth of crystalline CeO_2.

14. SUBJECT TERMS
atomic layer epitaxy (ALE), diamond, silicon carbide, CeO_2, conformal deposition, XPS, temperature programmed desorption, chlorinated methylsilanes, interfacial reaction

15. NUMBER OF PAGES
31

16. PRICE CODE

17. SECURITY CLASSIFICATION OF REPORT	18. SECURITY CLASSIFICATION OF THIS PAGE	19. SECURITY CLASSIFICATION OF ABSTRACT	20. LIMITATION OF ABSTRACT
UNCLAS	UNCLAS	UNCLAS	SAR

Table of Contents

I.	Introduction	1
II.	Atomic Layer Epitaxy of Silicon Carbide Thin Films	4
III.	Integrated Surface Science System for Atomic Layer Epitaxy of Silicon Carbide	13
IV.	Diamond Nucleation Using Halogenated Organosilicics	17
V.	Reaction and Regrowth Control of CeO_2 on Si (111) Surface for the Silicon on Insulator Structure	23
VI.	Distribution List	31

Accesion For
NTIS CRA&I ☒
DTIC TAB ☐
Unannounced ☐
Justification
By
Distribution /
Availability Codes
Dist | Avail and / or Special
A-1

DTIC QUALITY INSPECTED 3

I. Introduction

Atomic layer epitaxy (ALE) is the sequential chemisorption of one or more elemental species or complexes within a time period or chemical environment in which only one monolayer of each species is chemisorbed on the surface of the growing film in each period of the sequence. The excess of a given reactant which is in the gas phase or only physisorbed is purged from the substrate surface region before this surface is exposed to a subsequent reactant. This latter reactant chemisorbs and undergoes reaction with the first reactant on the substrate surface resulting in the formation of a solid film. There are essentially two types of ALE which, for convenience, shall be called Type I and Type II.

In its early development in Finland, the Type I growth scenario frequently involved the deposition of more than one monolayer of the given species. However, at that time, ALE was considered possible only in those materials wherein the bond energies between like metal species and like nonmetal species were each less than that of the metal-nonmetal combination. Thus, even if multiple monolayers of a given element were produced, the material in excess of one monolayer could be sublimed by increasing the temperature and/or waiting for a sufficient period of time under vacuum. Under these chemical constraints, materials such as GaAs were initially thought to be improbable since the Ga-Ga bond strength exceeds that of the GaAs bond strength. However, the self-limiting layer-by-layer deposition of this material proved to be an early example of Type II ALE wherein the trimethylgallium (TMG) chemisorbed to the growing surface and effectively prevented additional adsorption of the incoming metalorganic molecules. The introduction of As, however caused an exchange with the chemisorbed TMG such that a gaseous side product was removed from the growing surface. Two alternating molecular species are also frequently used such that chemisorption of each species occurs sequentially and is accompanied by extraction, abstraction and exchange reactions to produce self-limiting layer-by-layer growth of an element, solid solution or a compound.

The Type II approach has been used primarily for growth of II–VI compounds [1–13]; however, recent studies have shown that it is also applicable for oxides [14–18], nitrides [19], III–V GaAs-based semiconductors [20–33] and silicon [34–36]. The advantages of ALE include monolayer thickness control, growth of abrupt interfaces, growth of uniform and graded solid solutions with controlled composition, reduction in macroscopic defects and uniform coverage over large areas. A commercial application which makes use of the last attribute is large area electroluminescent displays produced from II–VI materials. Two comprehensive reviews [37,6], one limited overview [38] and a book [39] devoted entirely to the subject of ALE have recently been published.

The materials of concern in this program include silicon carbide (SiC), diamond (C) and cerium dioxide (CeO_2). Deposition of all three materials has been achieved using the

progressive decomposition of metal-organic precursors (SiC and diamond) and laser ablation (CeO_2). In addition, an XPS/Auger system has been commissioned to fully study the chemistry of the ALE growth cycle for SiC.

The following sections introduce each topic, detail the experimental approaches, report the results to date and provide a discussion and a conclusion for each material. Each major section is self-contained with its own figures, tables and references.

References

1. T. Suntola and J. Antson, U.S. Patent 4,058,430 (1977).
2. M. Ahonen, M. Pessa and T. Suntola, Thin Solid Films **65**, 301 (1980).
3. M. Pessa, R. Makela, and T. Suntola, Appl. Phys. Lett. **38**, 131 (1981).
4. T. Yao and T. Takeda, Appl. Phys. Lett. **48**, 160 (1986).
5. T. Yao, T. Takeda, and T. Watanuki, Appl. Phys. Lett. **48**, 1615 (1986).
6. T. Yao, Jpn. J. Appl. Phys. **25**, L544 (1986).
7. T. Yao and T. Takeda, J. Cryst. Growth **81**, 43 (1987).
8. M. Pessa, P. Huttunen and M.A. Herman, J. Appl. Phys. **54**, 6047 (1983).
9. C. H. L. Goodman and M. V. Pessa, J. Appl. Phys. **60**, R65 (1986).
10. M. A. Herman, M. Valli and M. Pessa, J. Cryst. Growth **73**, 403 (1985).
11. V. P. Tanninen, M. Oikkonen and T. Tuomi, Phys. Status Solidi **A67**, 573 (1981).
12. V. P. Tanninen, M. Oikkonen and T. Tuomi, Thin Solid Films **90**, 283 (1983).
13. D. Theis, H. Oppolzer, G. Etchinghaus and S. Schild, J. Cryst. Growth **63**, 47 (1983).
14. S. Lin, J. Electrochm. Soc. **122**, 1405 (1975).
15. H. Antson, M. Leskela, L. Niinisto, E. Nykanen and M. Tammenmaa, Kem.-Kemi **12**, 11 (1985).
16. R. Tornqvist, Ref. 57 in the bibliography of Chapt. 1 of Ref. 39 of this report.
17. M. Ylilammi, M. Sc. Thesis, Helsinki Univ. of Technology, Espoo (1979).
18. L. Hiltunen, M. Leskela, M. Makela, L. Niinisto, E. Nykanen and P. Soininen, Surface Coatings and Technology, in press.
19. I. Suni, Ref. 66 in the bibliography of Chapt. 1 of Ref. 39 in this report.
20. S. M. Bedair, M. A. Tischler, T. Katsuyama and N.A. El-Masry, Appl. Phys. Lett. **47**, 51 (1985).
21. M. A. Tischler and S. M. Bedair **48**, 1681 (1986).
22. M. A. Tischler and S. M. Bedair, J. Cryst. Growth **77**, 89 (1986).
23. M. A. Tischler, N. G. Anderson and S.M. Bedair, Appl. Phys. Lett. **49**, 1199 (1986).
24. M. A. Tischler, N. G. Anderson, R.M. Kolbas and S.M. Bedair, Appl. Phys. Lett. **50**, 1266 (1987).
25. B.T. McDermott, N. A. El-Masry, M. A. Tischler and S.M.Bedair, Appl. Phys. Lett. **51**, 1830 (1987).
26. M. A. Tischler, N. G. Anderson, R. M. Kolbas and S. M. Bedair, SPIE Growth Comp. Semicond. **796**, 170 (1987).
27. S. M. Bedair in Compound Semiconductor Growth Processing and Devices for the 1990's, Gainesville, FL, 137 (1987).
28. J. Nishizawa, H. Abe and T. Kurabayashi, J. Electrochem. Soc. **132**, 1197 (1985).
29. M. Nishizawa, T. Kurabayashi, H. Abe, and N. Sakurai, J. Electrochm. Soc. **134**, 945 (1987).
30. P. D. Dapkus in Ref. 27, p. 95.
31. S. P. Denbaars, C. A. Beyler, A. Hariz and P. D. Dapkus, Appl. Phys. Lett. **51**, 1530 (1987).
32. M. Razeghi, Ph. Maurel, F. Omnes and J. Nagle, Appl. Phys. Lett. **51**, 2216 (1987).

33. M. Ozeki, K. Mochizuki, N. Ohtsuka and K. Kodama, J. Vac. Sci. Technol. **B5**, 1184 (1987).
34. Y. Suda, D. Lubben, T. Motooka and J. Greene, J. Vac. Sci. Technol. **B7**, 1171 (1989).
35. J. Nishizawa, K. Aoki, S. Suzuki and K. Kikuchi, J. Cryst. Growth **99**, 502 (1990).
36. T. Tanaka, T. Fukuda, Y. Nagasawa, S. Miyazaki and M. Hirose, Appl. Phys. Lett. **56**, 1445 (1990).
37. T. Suntola and J. Hyvarinen, Ann. Rev. Mater. Sci. **25**, 177 (1985).
38. M. Simpson and P. Smith, Chem. Brit. **23**, 37 (1987).
39. T. Suntola and M. Simpson, Atomic Layer Epitaxy, Chapman and Hall, New York, 1990.

II. Atomic Layer Epitaxy of Silicon Carbide Thin Films

A. Introduction

With a high junction breakdown electric field of 5×10^6 V/cm [1], wide bandgap of 2.2 eV [2] and a high thermal conductivity of 3.5 w/cm°C at room temperature [3], SiC has great performance potential for many kinds of discrete and integrated devices. Specifically, the superior thermal, electrical and chemical properties of SiC are very appealing for producing high-speed, -power and -temperature devices. Indeed many types of devices with excellent records of performance have been fabricated in the laboratory [4]. However, at present, SiC is not found in many commercial device applications. A substantial barrier to the wider use of devices made from this material is the lack of a technology that allows the incorporation of a SiC thin film processing route into the existing Si device and integrated circuit infrastructure.

Although all of the common polytypes of SiC: 2H, 4H, 6H and 3C exhibit physical properties that are attractive for devices, the lone cubic polytype, 3C or β-SiC, is most appealing. In addition to a predicted drift velocity that is slightly higher than the other polytypes due to reduced phonon scattering [5], this polytype has the advantage that it can be deposited epitaxially on Si substrates. Typically, monocrystalline deposition of SiC on a Si(100) substrate occurs in two steps. Firstly, an off-axis wafer is exposed to a C-containing species to carbonize the surface to a thickness of 150–300Å. This SiC conversion layer is subsequently exposed to both Si- and C- containing gases at ≈1350°C to form much thicker cubic films [6]. Neither the carbonizing nor the high temperature steps can be easily integrated into current sub-micron Si process routes. However, atomic layer epitaxy offers the ability to eliminate both process difficulties and may enable the more widespread use of SiC in selected devices.

The objective of this research is to extend the state-of-the-art regarding SiC thin film deposition and application via the employment of Atomic Layer Epitaxy (ALE) to deposit β-SiC films on select substrates. During this reporting period, groundwork was performed to support the fabrication of trenched heterojunction bipolar transistors employing a wide bandgap β-SiC emitter. This work has included the deposition of SiC films within trenches etched into Si(100) substrates and the electrical characterization of unintentionally n-type and Al doped p-type monocrystalline β(3C)-SiC(100) films. The following sections describe the experimental procedures and the results and provide a discussion and conclusions regarding the research conducted in this period.

B. Experimental Procedure

ALE Reactor. The ALE reactor employed in this research has not been significantly modified since it was described in detail in the previous report (June 1993). To prevent mixing of process gases, flowing Ar "curtains" divide the reactor into 4 quadrants through

which isolated fluxes of Si_2H_6, C_2H_4, NH_3 and tiethylaluminum ($Al(C_2H_5)_3$) may flow. The quadrant containing NH_3 also contains a W filament that may be heated to produce atomic hydrogen or to crack NH_3 depending on gas flow conditions. During deposition, heated samples can be rotated alternately between quadrants and exposed to the species present to form films in a layer-by-layer process. Due to the construction of the reactor, SiC films can be deposited and doped n and p-type with N and Al, respectively.

Preparing Flat Substrates. Three kinds of wafer substrates were employed in this research: As doped (10^{19} cm^{-3}), n-type Si(100) oriented off-axis 3° toward <110>; B doped (10^{17} cm^{-3}), p-type Si(100); and N doped (10^{17} cm^{-3}), n-type α-6H-SiC(0001) oriented off-axis 3.5° toward $<11\bar{2}0>$. The α-6H-SiC(0001) substrates were received with ≈750 Å of SiO_2 grown on the surface so these substrates were immersed in a 10% HF solution for 5 minutes before loading into the system. Si(100) substrates were loaded into the system immediately after RCA cleaning.

Trenched Si(100) Substrates. Trenched Si substrates were produced from the n-type Si(100) wafers using conventional semiconductor fabrication techniques. Wafers were thermally oxidized according to a dry-wet-dry recipe at 950°C to form ≈5000 Å of SiO_2 which was photolithographically patterned using a custom mask. A series of parallel strips of Si were uncovered by dipping in HF. Using the SiO_2 pattern, the wafers were reactive ion etched at 100 watts in an atmosphere formed by flowing 15 and 12.5 sccm of SF_6 and O_2, respectively. The remaining SiO_2 was removed using an HF dip.

P-type SiC(100) Films. The Al dopant for the deposition of p-type β-SiC films was obtained from a conventional organometallic bubbler containing triethylaluminum (TEAl). During deposition the TEAl was held at 62°C, creating a vapor pressure of 1 Torr, and entrained in H_2 flowing at 150 sccm as the total bubbler pressure was maintained at 300 Torr.

Deposition. Silicon carbide films were deposited on the substrates by a sequential exposure to Si_2H_6, C_2H_4 and atomic hydrogen. The deposition of p-type films was accomplished by exposing the sample to a very dilute flow of TEAl between each Si and C exposure. Optimal growth conditions were a sample temperature of 850°C, a flow rate of ≈1 sccm for each source gas and an exposure to atomic hydrogen for 30 seconds after each Si-C cycle. The atomic hydrogen was produced by flowing 100 sccm of H_2 across a tungsten filament heated to ≈1800°C.

C. Results

Trenched Substrates. Several 3" diameter Si(100) wafers have been fabricated with parallel trenches running in the {110} direction. The trenches were fabricated in widths of approximately 7, 15, 35, and 50 μm and to a depth of 10μm giving a range of aspect ratios. Scanning electron microscopy has been used to observe the trenched substrates. A section of

a trenched substrate is shown in Fig. 1 and a higher magnification view of a single trench is shown in Fig. 2.

Uniform monocrystalline β-SiC(100) films were deposited on the trenched Si(100) wafers. Figure 3 is a scanning electron microscopy (SEM) image of a 0.2 μm thick SiC film deposited within a trench measuring 7 μm across and 10 μm deep. Uniform coverage is evident within the trench. A higher magnification view of another film in Fig. 4 indicates the excellent conformality of the film over surface irregularities.

Electrical Properties. N- and p-type films grown on substrates of the opposite conductivity type have been examined based on Hall mobility and I-V behavior. Undoped films were n-type with carrier concentrations of approximately 10^{18} cm^{-3} and mobilities of ≈ 400 $cm^2V^{-1}s^{-1}$. P-type films had carrier concentrations of $\approx 10^{19}$ cm^{-3} and mobilities of ≈ 20 $cm^2V^{-1}s^{-1}$. Diodes have been constructed with the p-type films on n type substrates as depicted in Fig. 5. Rectifying behavior was observed, but the junctions were leaky with reverse currents at -10 volts of 5 10^{-5} amperes/ cm^2.

D. Discussion

Deposition Process. Through judicious selection of process variables, it was possible to "dose" substrates with an amount of each process gas sufficient to deposit approximately one monolayer of each species per deposition cycle. In this manner a growing SiC film was first covered with Si and then converted to SiC upon exposure to C_2H_4. The latter step was followed by an exposure to atomic hydrogen that served to remove any excess C on the surface and very likely increased the surface mobility of the Si and C species. This was supported by the observation of improved crystallinity, as indicated by RHEED, as the C exposure was reduced from 10 to 1.5 times the Si exposure with all other parameters held constant. This trend is elucidated in Fig. 6 where the C_2H_4 flow rate was varied from 2 to 6 sccm as all other process variables were held constant. It can be seen that the quality of the film is optimized at a flow rate of 4 sccm. In addition, the required residence time below atomic hydrogen to form monocrystalline films decreased with reduced C exposure.

Although HRTEM indicated that the films contained <111> twins and stacking faults as seen in Fig. 7, continued optimization of process variables has allowed the deposition of improved SiC films.

While the ability to deposit n-type films uniformly within trenches has been demonstrated, p-type films were less uniform within trenches, exhibiting significant shadowing as seen in Figure 8. This may be due to incomplete decomposition of the TEAl molecule used as a dopant. Any carbon remaining attached to the Al impinging the substrate surface may react with surface Si, halting surface migration. Further optimization of this process is required to allow more flexibility in device structures.

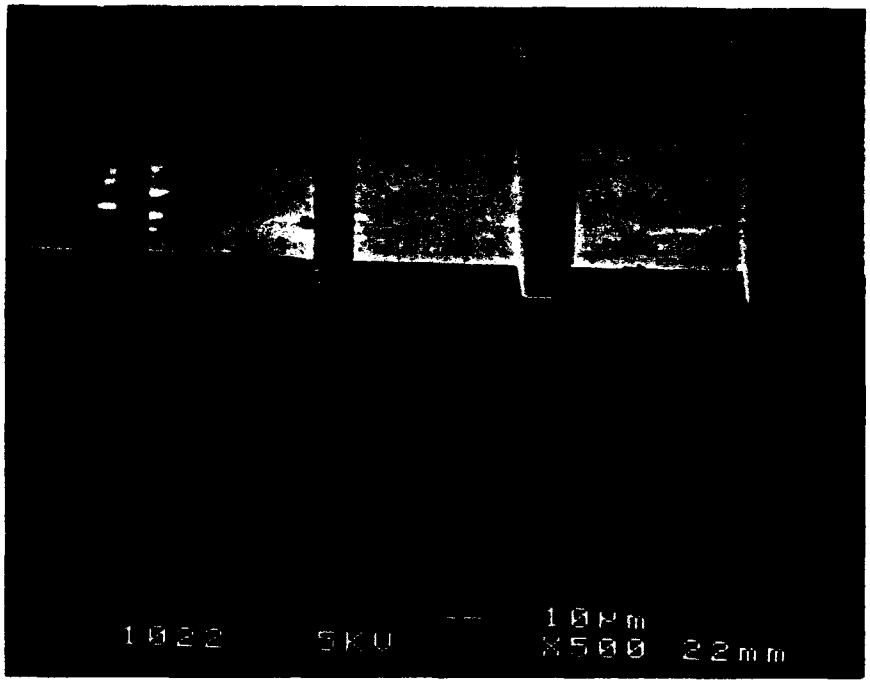

Figure 1. Trenches in Si(100) substrate.

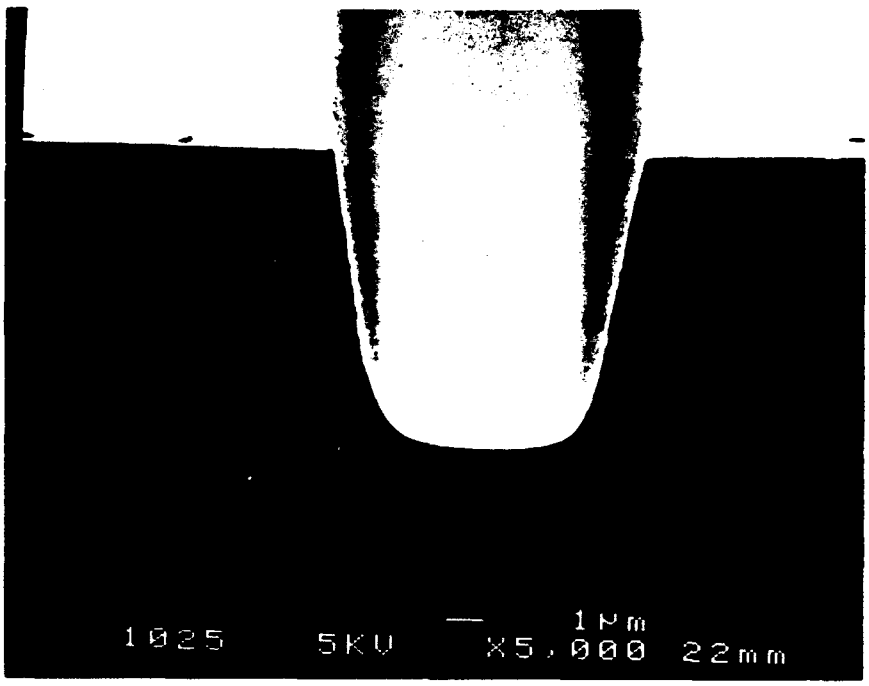

Figure 2. High magnification view of a trench.

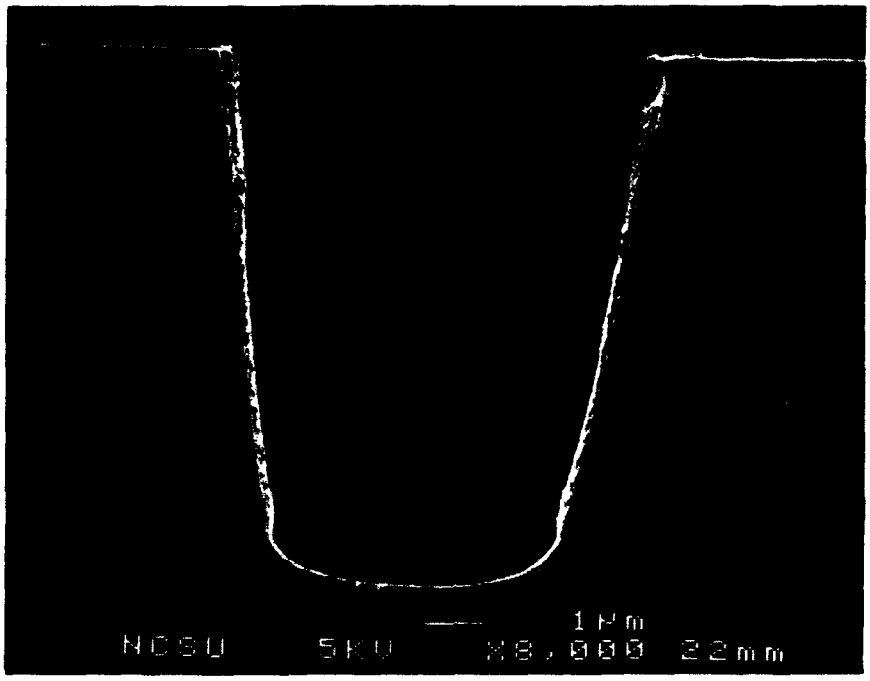

Figure 3. SiC film on trenched Si(100) substrate.

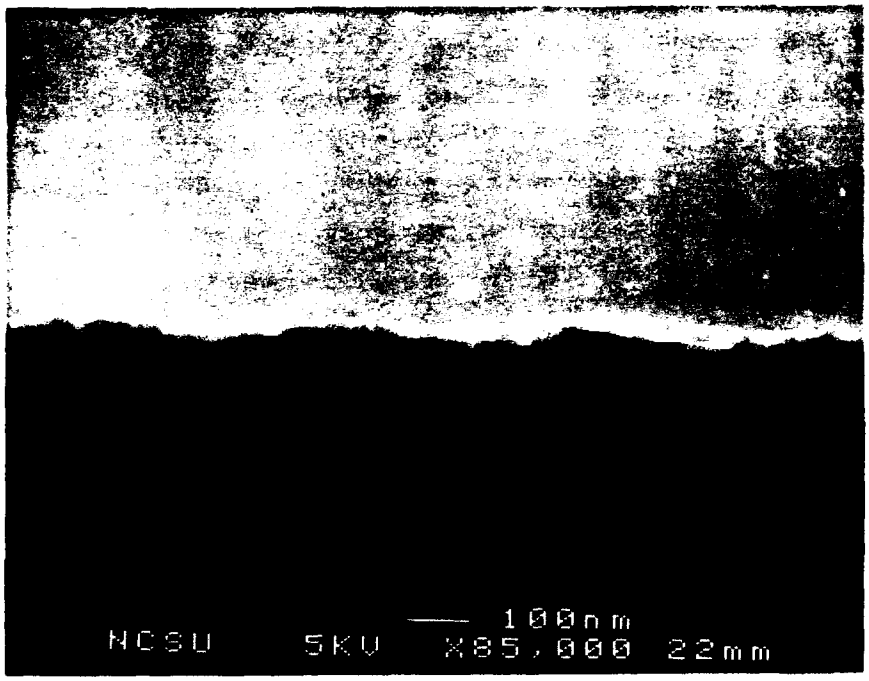

Figure 4. High magnification view of film in trench.

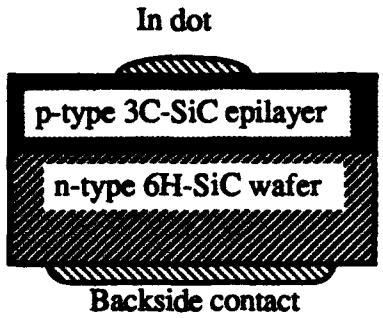

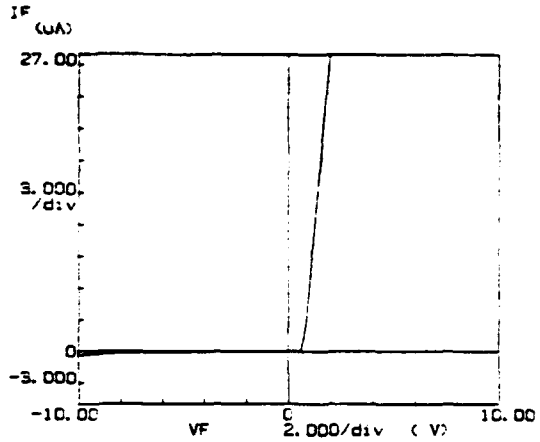

Figure 5. Structure and behavior of diode fabricated with p-type SiC ALE layer. Dot size $\approx 7\times10^{-3}$ cm^2.

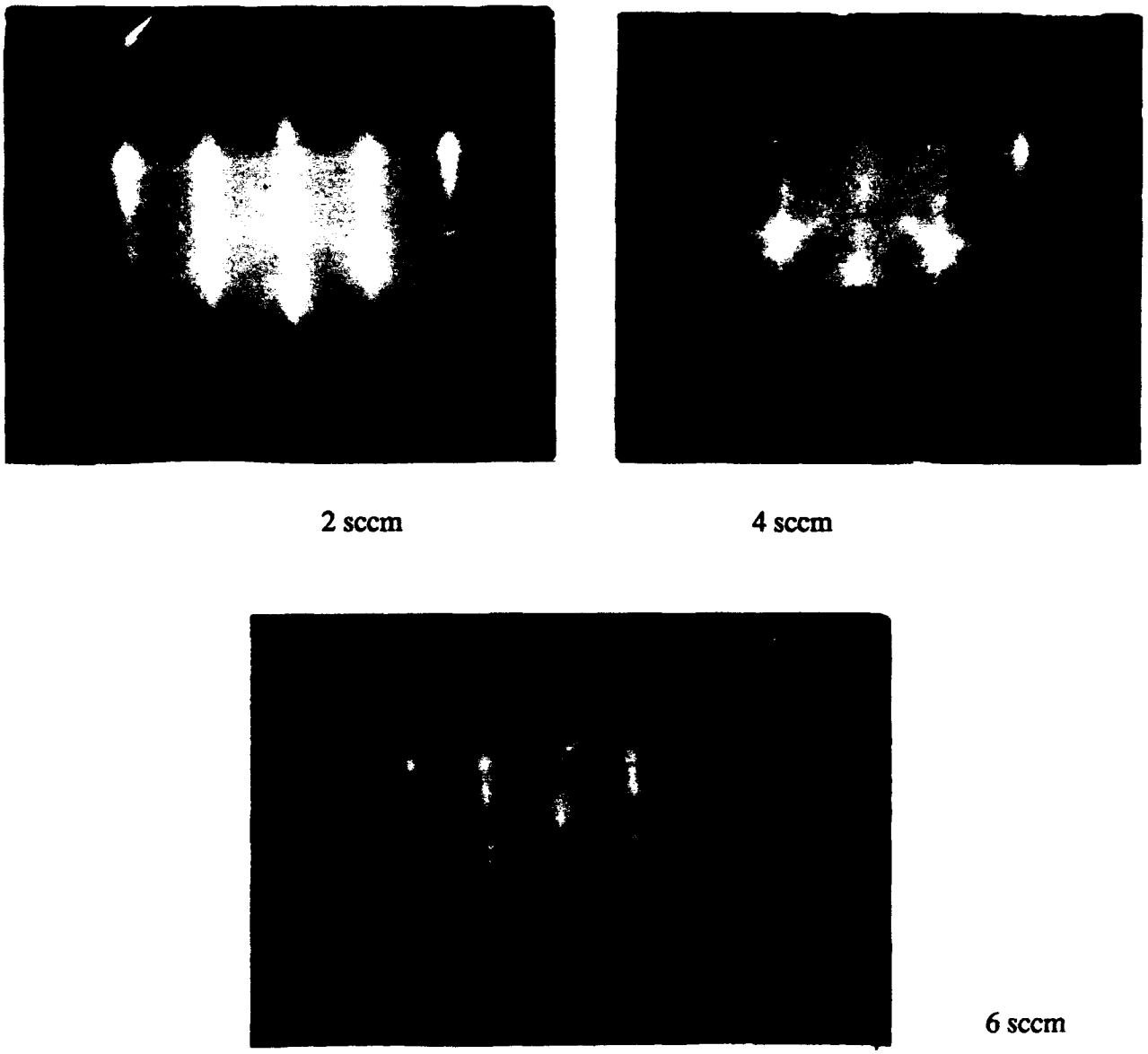

Figure 6. Crystallinity of SiC deposited on SiC substrate dependent on C_2H_4 dose.

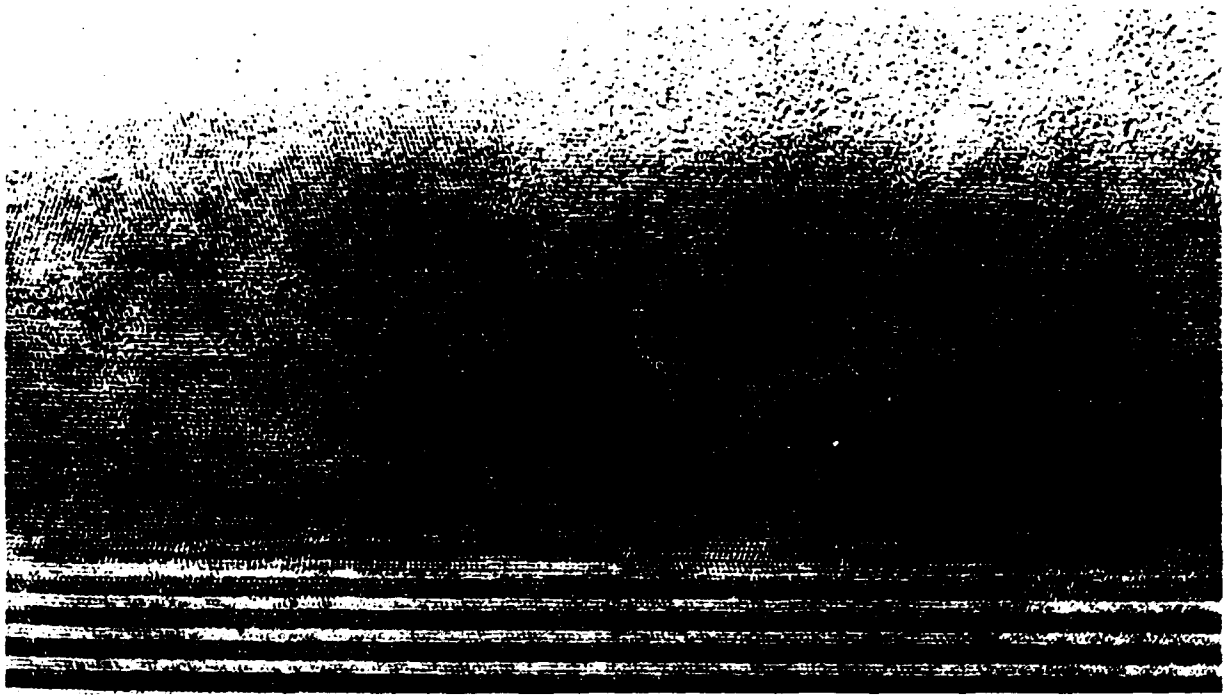

Figure 7. HRTEM image of 3C-SiC film on 6H-SiC substrate.

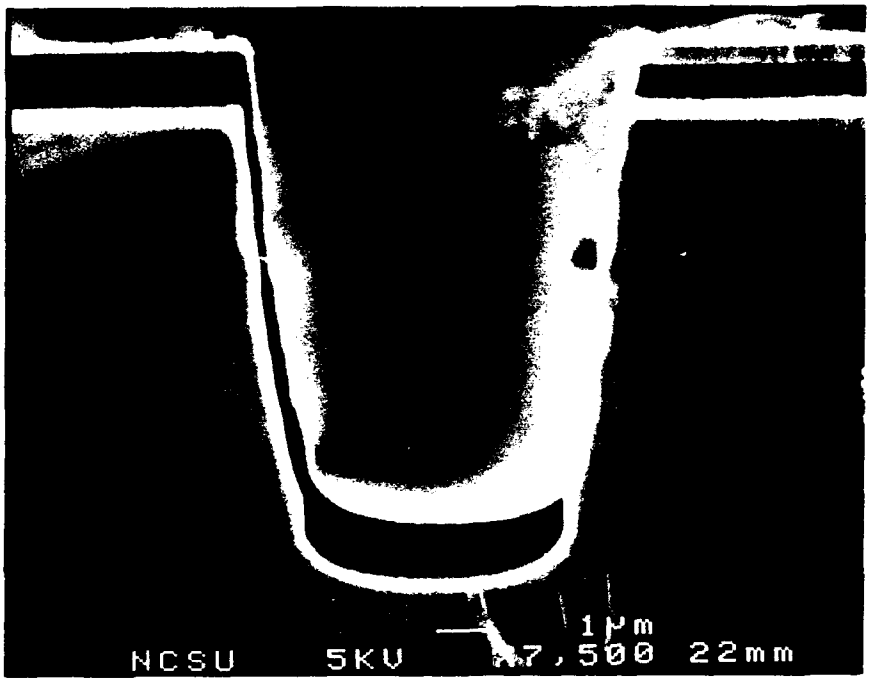

Figure 8. P-type 3C-SiC film on trenched Si(100) wafer.

The ability to dope SiC films n and p-type during ALE growth has been demonstrated. A significant problem remaining to be solved is the reduction of the unintentional n-type doping of the films.

E. Conclusions

Using a cyclic layer-by-layer technique we have demonstrated the feasibility for deposition of very uniform β-SiC(100) films on flat and trenched Si substrates at 850°C without employing a preliminary carbonization step. N and p-type films of β-SiC have been deposited with the n-type films exhibiting a Hall mobility of ≈400 $cm^2V^{-1}s^{-1}$ at n= 10^{18} cm^{-3} while p-type films having hole mobilities of ≈20 $cm^2V^{-1}s^{-1}$ at p=10^{19} cm^{-3}. Rudimentary SiC diodes have been fabricated and tested. These are necessary steps toward employing the ALE technique for integrating β-SiC into conventional Si device processing.

F. Future Research Plans

1. Reduce unintentional n-type doping of SiC films.
2. Develop better control over n and p-type doping.
3. Develop trench heterojunction bipolar transistors using β-SiC emitters.

As a vertical power device, the bipolar transistor has advantages over field effect transistors (FETs) when incorporated to densely packed integrated circuits. Almost the entire bipolar device carries current unlike the FET where all of the current flows through a relatively narrow channel. This difference in operation gives the bipolar device its high power and speed advantages. When a wide bandgap emitter is employed to make a heterojunction bipolar transistor, the performance of the bipolar device is further enhanced by the higher energy of carriers injected into the base region giving shorter transit times and allowing higher base doping to reduce the extrinsic base resistance, both improving the devices speed. With the current premium placed on i.c. real estate, building the HBTs in trenches would also add to the device's appeal. ALE offers a mechanism to produce trench HBTs with β-SiC emitters on Si(100) wafers.

Figure 9 depicts the HBT structure being developed at this time. The device is a mesa isolated n^+-p-n device constructed on a n^+ Si(100) wafer to allow a backside contact without high collector losses. Contacts are expected to be sputtered Pt which should be ohmic on the highly doped emitter and wafer while a small barrier is expected at the more lightly doped base region. Although the base region doping is sub optimal for a wide bandgap emitter, the selection of the doping level should allow the fabrication devices with monocrystalline Si and polysilicon emitters for bipolar device comparison and allow forming HBTs with amorphous silicon emitters for wide bandgap emitter comparison.

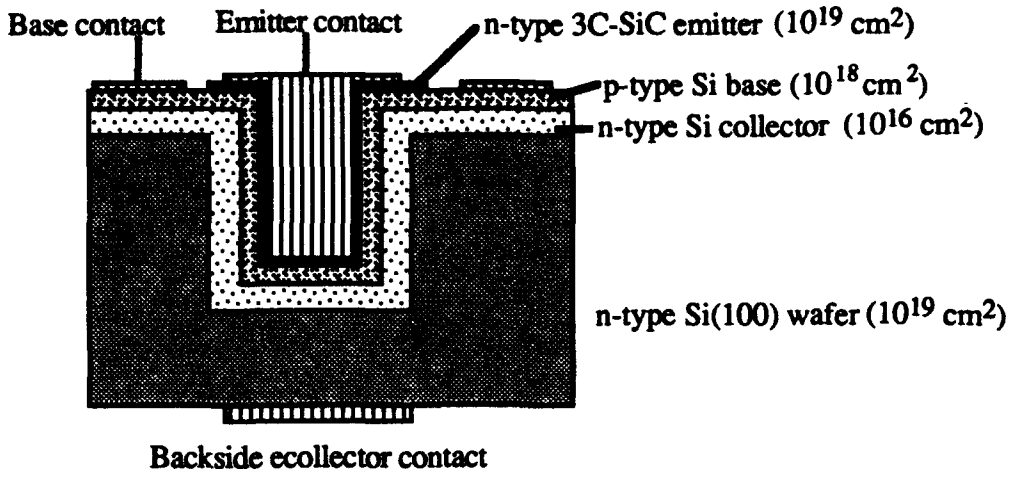

Figure 9. Current trench HBT design.

G. References

1. W. von Muench and I. Pfaffender, J. Appl. Phys. **48**, 4831 (1977).
2. N. W. Jepps and T. F. Page, "Polytypic Transformations in Silicon Carbide" in *Progress in Crystal Growth and Characterization, Crystal Growth and Characterization of Polytype Structures*, P. Krishna, Ed., Pergamon, NY, (1983), pp. 259-307.
3. E. A. Bergemeister, W. von Muench and E. Pettenpaul, J. Appl. Phys. **50**, 5790 (1979).
4. R. F. Davis, G. Kelner, M. Shur, J. W. Palmour and J. A. Edmund, *Proceed. IEEE* **79**, 677 (1991).
5. P. Das and D. K. Ferry, Solid State Electron. **19**, 851 (1976).
6. H. P. Liaw and R. F. Davis, J. Electrochem. Soc. **131**, 3014 (1984).

III. Integrated Surface Science System for Atomic Layer Epitaxy of Silicon Carbide

A. Introduction

In this report period, efforts have focused on fine tuning the analytical capabilities of the integrated ALE systems while simultaneously studying the available cleaning methods for Si and SiC. In the case of silicon, TPD (temperature programmed desorption) has been used to look at the hydrogen plasma cleaning of silicon (100) wafers. Hydrogen plasma cleaning of SiC has also been attempted and in this case, XPS (x-ray photoelectron spectroscopy) shows that residual hydrocarbons and fluorine can be removed.

B. Experimental Procedure

Substrate Cleaning. All wafers (Si (100) and 6H-SiC) are given a standard UV-HF spin treatment prior to insertion into vacuum. Once *in vacuo*, Si and SiC are hydrogen plasma cleaned using various times and temperatures in a RF plasma system described elsewhere [1]. XPS and LEED is generally performed both before and after plasma cleaning to asses the removal of hydrocarbons, fluorine, and oxygen. TPD is performed after plasma cleaning as a check for hydrogen termination and the amount of subsurface hydrogen in the wafer.

C. Results and Discussion

Plasma cleaning of Si (100). TPD was performed on silicon wafers which had been hydrogen plasma cleaned using a variety of different conditions which are: 150°C–2min., 150°C–1hr., 450°C–2min., and 450°C–1hr. After plasma cleaning, all wafers exhibited a (1×1) LEED pattern indicative of a dihydride silicon surface. The one characteristic feature common to all four wafers in the TPD spectra was the continuous rise in pressure with temperature which never came back down to the background level, see Fig. 1. This continuous rise in pressure is attributed to subsurface hydrogen escaping from the silicon wafer. TPD spectra taken one day later on the same wafer shows little H_2 evolution indicating that this continuous evolution of H_2 is not a result of the sample heater.

TPD spectra of the wafers cleaned at 150°C (2min and 1hr) show similar peaks which can tentatively be attributed to the β_1, β_2, and β_3 hydrogen desorption states, see Fig. 1. The LEED patterns of these surfaces after TPD were both (2×1) indicating that all hydrogen was desorbed from the surface leaving behind a clean reconstructed surface.

The TPD spectra for the 450°C–1hr. wafer showed no characteristic features up to 625°C where the H_2 signal rapidly increased. AES (auger electron spectroscopy) of this surface showed that a surface oxide had been grown during plasma cleaning indicating the fact that the surface was not terminated with hydrogen. TPD of the 450°C–2min. surface yielded results intermediate to those previously detailed.

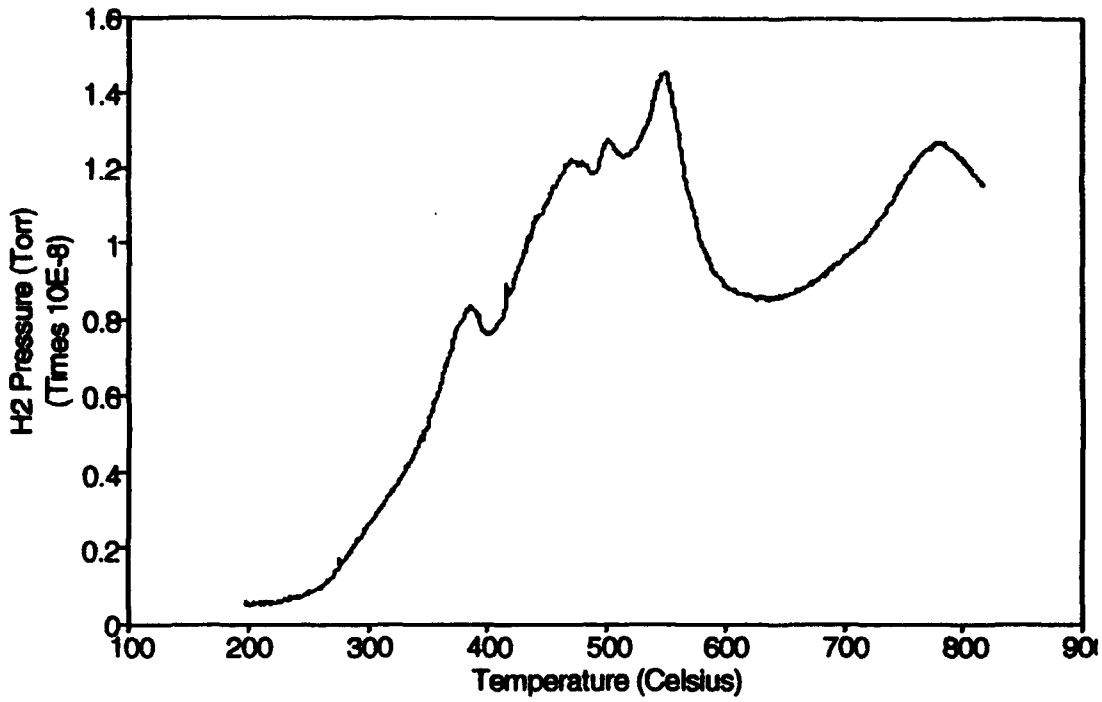

Figure 1. TPD spectra of a hydrogen plasma cleaned silicon (100) wafer: 150°C–1hr.

Plasma Cleaning of 6H-SiC (0001). XPS has been used to look at the hydrogen plasma cleaning of 6H-SiC (0001). Figure 2 shows an XPS spectrum of a 6H-SiC Cree Research, Inc. wafer cleaned in a RF hydrogen plasma at 650°C for 90 min. Aside from some surface oxide, the plasma effectively removed residual hydrocarbons, fluorine, etc. from the surface. This is illustrated more effectively in Fig. 3 which shows the C 1s peak of the SiC wafer in various stages of cleaning. The upper XPS scan corresponds to the wafer prior to any cleaning whatsoever. Two peaks are readily apparent with the one at 284 eV corresponding to carbon in SiC and the one at 285 eV to residual hydrocarbons. The middle scan in Fig. 3 shows the C 1s peak after the SiC wafer had been subjected to a UV-HF spin treatment. This treatment removes the residual hydrocarbons but still leaves some oxygen and fluorine at the surface bonded to the carbon in silicon carbide as evidenced by the high energy tail on the C 1s peak. The lower scan in Fig. 3 shows the SiC wafer after plasma cleaning at 650°C for 90 minutes. As can be seen, residual C-O and C-F bonding has been removed from the surface as witnessed by the loss of the high energy tail. Attempts are currently being made at cleaning 6H-SiC at lower temperatures and shorter times. The results to date are intermediate to the ones described above.

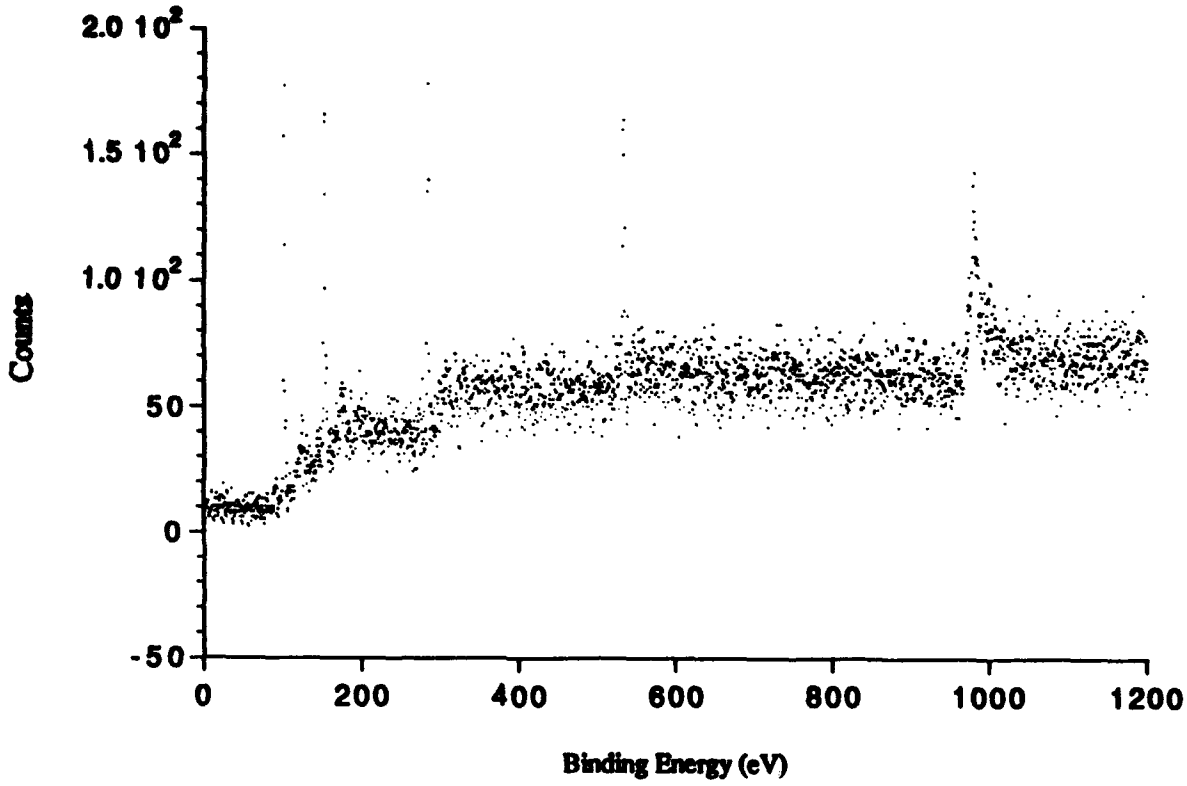

Figure 2. XPS survey scan of 6H-SiC wafer cleaned by hydrogen plasma at 650°C for 90 min.

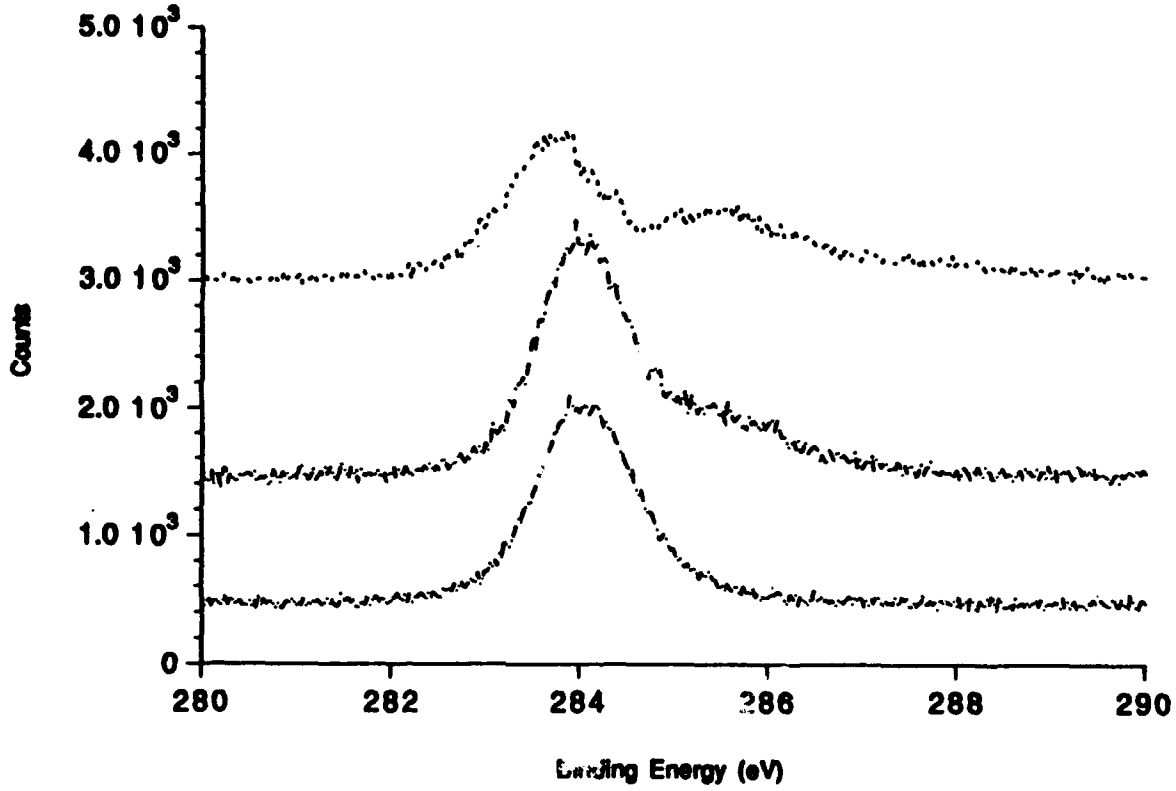

Figure 3. XPS Carbon 1s of 6H-SiC wafer after various stages of cleaning. Upper scan - no cleaning, Middle scan - after UV-HF spin, Lower scan - after plasma cleaning.

D. Conclusion

The effects of hydrogen plasma cleaning on silicon and silicon carbide have been investigated using TPD and XPS. The XPS studies show that hydrogen plasma cleaning is efficient at removing C-C, C-O, and C-F bonding at the silicon carbide surface. TPD studies of hydrogen plasma cleaned silicon and silicon surfaces indicates that the while terminating the surface with hydrogen lots of subsurface hydrogen is produced as well.

E. Future Research

The next step (and one of the main goals) in this research is to look at the adsorption of Si_2Cl_6 on Si (100) and SiC (0001). As detection of adsorbed silicon on silicon is not easily achieved using XPS, initial experiments have been performed on the adsorption of Si_2Cl_6 on Ge (100). While these experiments have not yet reached a stage suitable for presentation, they are necessary to test and characterize the Si_2Cl_6 dosing system. Once these studies on Ge (100) are complete, work will move on to looking at the adsorption of Si_2Cl_6 on both hydrogen terminated Si (100) and 6H-SiC (0001) using TPD, XPS, and LEED. Further studies will look at the adsorption of C_2H_2 on chlorine terminated Si (100) and SiC (0001).

F. Acknowledgements

John Barnak, Tom Schneider, and Professor Robert Nemanich for the use and assistance in the hydrogen plasma cleaning of silicon and silicon carbide.

G. References

1. T. P. Schneider, J. Cho, J. Vander Weide, S. E. Wells, G. Lucovsky, R. J. Nemanich, M. J. Martin, R. A. Rudder, R. J. Markunas, Mat. Res. Soc. Symp. Proc. **204**, 333 (1991).

IV. Diamond Nucleation Using Halogenated Organosilicics

A. Introduction

This report describes recent experiments involving the use of chlorine substituted organosilicic reagents for use as precursors in the atomic layer nucleation of diamond. In these experiments, four halogenated species, $(CH_3)_{4-x}SiCl_x$ (x = 0 to 3), are introduced onto cleaned and passivated single crystal silicon <111> substrates in a hot filament chemical vapor deposition (HFCVD) reactor in order to observe the effect of the increasing halogenation on subsequent diamond nucleation. After diamond nucleation, the resulting films are characterized by SEM and Raman spectroscopy.

B. Experimental Procedure

Single crystal Si <111> wafers are spin etched[1] and loaded into a HFCVD chamber fitted with a resistively heated sample stage. The chamber is purged with argon and quickly pumped down to 5×10^{-5} torr. Helium carrier gas flow is started and the chamber pressure is maintained typically at 5 torr. The sample is then heated with the stage to 600 °C. Five microliters of reagent are injected into the carrier gas flow via a syringe injection system. Sufficient time is allowed for the species to react with the substrate. Then the helium flow is terminated and bias enhanced HFCVD of diamond using 2% CH_4/H_2 is performed on the treated substrate for a period of 20 minutes. SEM and Raman spectroscopy are used to evaluate the diamond nucleation density and quality.

C. Results

Figure (1a) and (1b) show scanning electron micro graphs of diamond films grown on Si wafers treated with $(CH_3)_2SiCl_2$ and CH_3SiCl_3, respectively. The nucleation densities of these films were measured to be 2.6×10^9 cm^{-2} in (1a) and 1.0×10^9 cm^{-2} in (1b). The films grown on wafers treated with $(CH_3)_4Si$ and $(CH_3)_3SiCl$ were similar in morphology and texture. Table I lists the measured diamond nucleation densities for the films grown with the four precursors.

Table I. Diamond nucleation densities for treated substrates.

Precursor	particles/cm^2
$(CH_3)_4Si$	2.0×10^9
$(CH_3)_3SiCl$	3.0×10^9
$(CH_3)_2SiCl_2$	2.6×10^9
CH_3SiCl_3	1.0×10^9

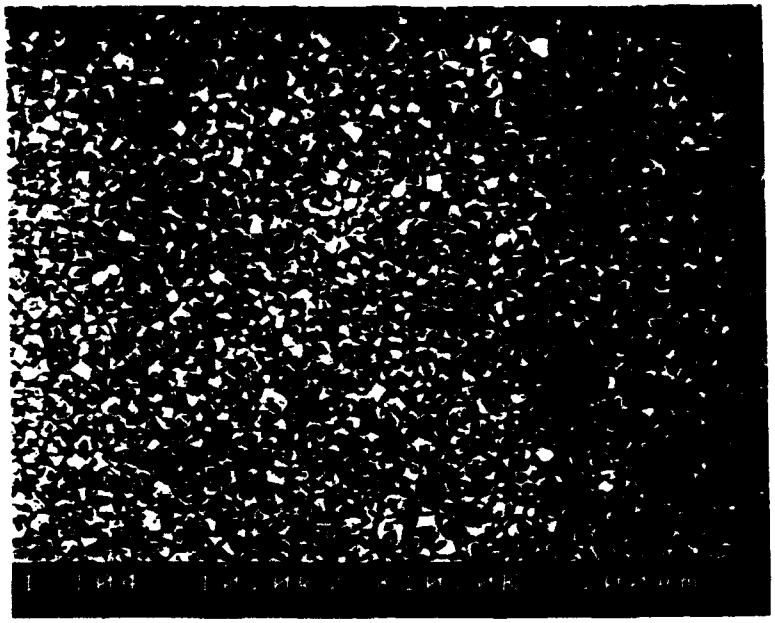

(a)

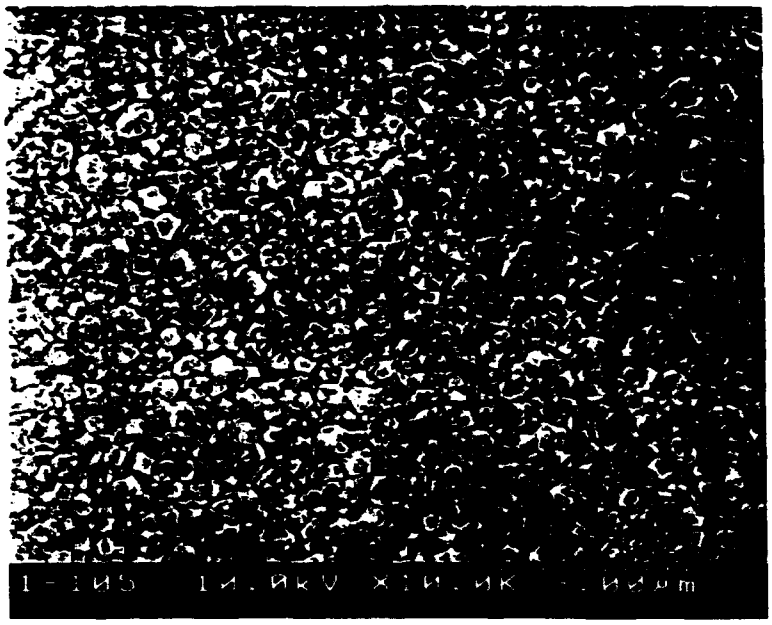

(b)

Figure 1. SEM micrographs of diamond films on Si <111> substrates treated with (a) $(CH_3)_2SiCl_2$ and (b) CH_3SiCl_3.

Fig. 2 shows the Raman spectra for the four films. The spectrum for the $(CH_3)_2SiCl_2$ treated wafer shows a sharp peak at 1334 cm^{-1}, slightly shifted from the characteristic diamond peak at 1332 cm^{-1}. There are sharp peaks at 1332 cm^{-1} for the other three films, however, a large graphitic component is present in all four spectra.

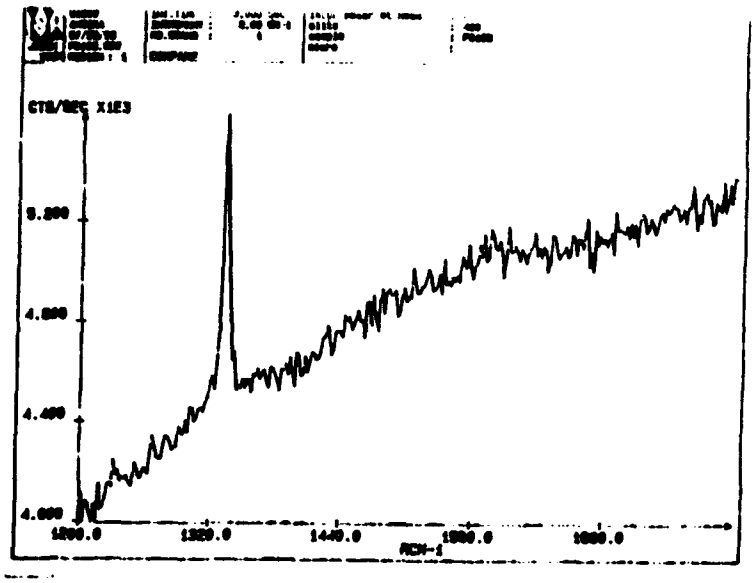

$(CH_3)Cl_3Si$

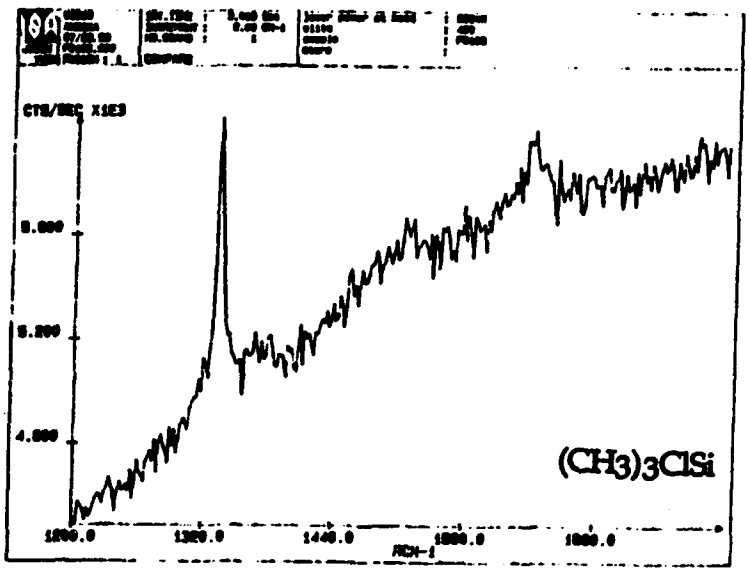

$(CH_3)_3ClSi$

Figure 2. Raman spectra of diamond films on treated Si <111> substrates.

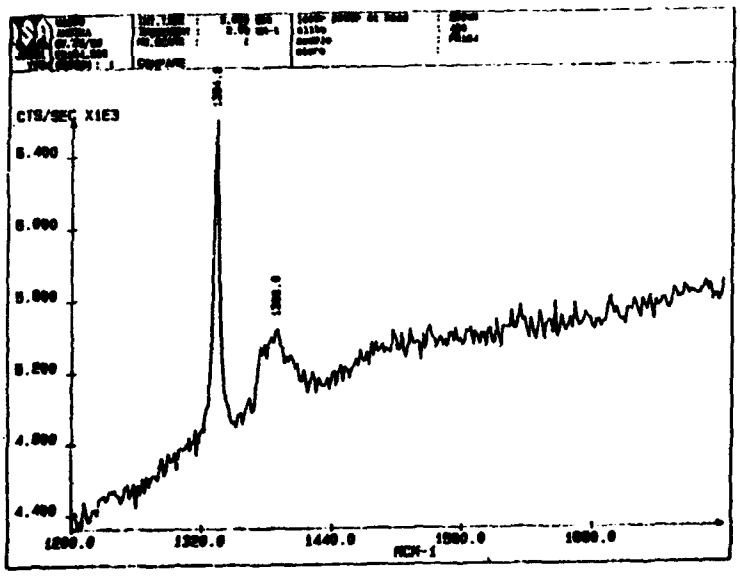

$(CH_3)_2Cl_2Si$

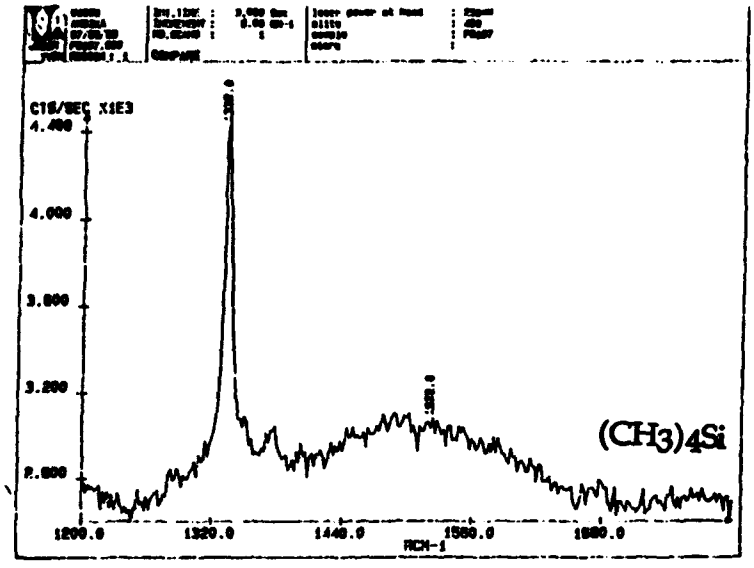

$(CH_3)_4Si$

Figure 2. Continued: Raman spectra of diamond films on treated Si <111> substrates.

D. Discussion

These experiments were designed to investigate the influence on diamond nucleation of decreasing the number of methyl groups on the $(CH_3)_4Si$ molecule by substituting chlorine for methyl groups. Since the Si-Cl bond energy (406 kJ/mol) is less than the Si-CH_3 bond energy (451 kJ/mol), Cl will leave before the methyl group. We expected that the more highly Cl substituted molecules would bond more easily with the Si substrate surface since the loss of the chlorine's would leave Si dangling bonds available to bond with the Si substrate. The results indicated, however, that there was no significant difference in subsequent diamond nucleation density. One reason for this result may be that the methyl hydrogen's are leaving, allowing methyl carbons to bond to the silicon substrate resulting in an amorphous carbon surface. This reasoning is supported by the amorphous peaks in the Raman spectra. Another reason may be contamination by oxygen during the syringe injection procedure since it is difficult to completely remove oxygen from the interior of the gas syringe and the halogenated methyl silanes are getter oxygen [2].

E. Conclusions

Experiments investigating the use of chlorinated methylsilanes as diamond precursors were conducted. These precursors were introduced onto cleaned and passivated Si <111> substrates, which were then subjected to bias enhanced HFCVD diamond growth conditions. Characterization by SEM and Raman spectroscopies revealed no significant difference in diamond nucleation density or quality between precursor species. Two possible causes of this result are the unintentional cleavage of methyl hydrogen's resulting in the methyl carbon bonding to the substrate and oxygen contamination during syringe injection of the liquid organometallics.

F. Future Work

A solution to both of the above mentioned difficulties is to use methyl silane, CH_3SiH_3, as a precursor. Since methyl silane is gaseous, it will be possible to introduce it into the HFCVD chamber without the possibility of oxygen contamination. Secondly, the H-SiH_2CH_3 bond energy (375 kJ/mol) is significantly less than either the H-CH_2 bond strength (460 kJ/mol), or the Si-CH_3 bond strength (451 kJ/mol). This lower bond energy will allow the molecule to decompose via dehydrogenation of the H-Si hydrogen's, without allowing the methyl hydrogen's to leave and cause carbon to bond to the substrate surface. A cylinder of methyl silane has been purchased, and we are now in the process of installing the required piping into our HFCVD chamber.

G. References

1. D. B. Fenner, D. K. Biegelsen, and R. D. Bringans, Journal of Applied Physics **66** (1), 419 (1989).
2. L. H. Dubois, R. G. Nuzzo, Surface Science **149**, 133 (1985).

V. Reaction and Regrowth Control of CeO_2 on Si (111) Surface for the Silicon on Insulator Structure

T.Chikyow [a,c], L. Tye [b], N.A. El-Masry [b] and S.M.Bedair [a]

a) *Electrical and Computer Engineering, North Carolina State University,*

Box 7911 Raleigh North Carolina 27695-7911

b) *Materials Science and Engineering, North Carolina State University,*

Box 7911, Raleigh North Carolina 27695-7911

c) *on leave from National Research Institute for Metals, Tsukuba Laboratories,*

1-2-1 Sengen Tsukuba-shi Ibaraki 305 JAPAN

PACS NUMBERS : 68.35.-P, 61.16.Di, 68.35.Rh

Abstract

An interface structure of CeO_2/Si (111) grown by laser ablation in ultra high vacuum was investigated by high resolution transmission electron microscopy and Auger electron spectroscopy. The deposited film was single crystalline CeO_2, as indicated by RHEED and x-ray diffraction observations. During the deposition, a reaction between CeO_2 and Si occurred at the interface. This reaction resulted in the formation of an oxygen deficient amorphous CeO_x layer and a SiO_2 layer. Post annealing in oxygen atmosphere caused the disappearance of the amorphous CeO_x and the regrowth of crystalline CeO_2. The SiO_2 thickness was also increased by annealing. The modified structure of CeO_2/SiO_2/Si is expected to be useful for the silicon on insulator structure.

Submitted to Applied Physics Letters

The Silicon on insulator structure (SOI) is a promising structure for high speed devices [1]. The SOI structure requires a thin epitaxial Si layer with low defect density and a buried insulator with high endurance voltage for the expected performances [2]. In the past, various types of SOI structure were proposed and demonstrated. They include lateral growth of amorphous Si [3], regrowth of amorphous Si by laser annealing [4], separation by implanted oxygen (SIMOX) [5] and direct wafer bonding [6,7] . However, these approaches have some difficulties, such as defect generation [8,9] control of regrowth orientation, [10] and uncertainty of the thickness of the insulating layer [7].

The idea of using a crystalline insulator seems to be preferable from the viewpoint of crystalline quality and thickness control of the epitaxial Si layer [11]. One approach was the combination of single crystalline spinel ($MgO+Al_2O_3$) on Si (100), followed by oxidation [14,15]. A serious problem in this method is the large lattice mismatch between spinel and Si [14]. Another candidate for crystalline insulator for SOI was CaF_2, which has a close lattice parameter to Si. However, a reaction reportedly occurs at the CaF_2/Si interface, leading to contamination of the interface region with Ca atoms [15,16].

Recently, CeO_2 has gained much attention as a promising crystalline insulator. It has a CaF_2 structure and the lattice mismatch of CeO_2 to Si is estimated to be 0.35%, which is better than the mismatch between CaF_2 and Si [17,18]. The dielectric constant of CeO_2 is ≈ 26, which makes it attractive as a capacitor material for dynamic random access memory. Epitaxial growth of CeO_2 on Si was already reported [18,19]. Potential applications will depend on better understanding and controlling the quality of the CeO_2/Si interface.

In this letter, the interfacial structure of CeO_2/Si (111) is investigated in detail by high resolution transmission electron microscopy and Auger electron spectroscopy. Based on observation and analysis, post annealing in oxygen atmosphere is carried out to modify the structure to CeO_2/SiO_2/Si (111) with the expectation of improving the insulating properties of the film for SOI applications.

P-type Si (111) wafers with 0.5 ohm-cm resistance were used as substrates. After the degreasing process, the wafer was dipped in a hot solution of NH_4OH : H_2O_2: H_2O (=1:1:6) followed by a dip in diluted HF and a rinse in deionized water. Subsequently the wafers were soaked in a hot solution of $HCl:H_2O_2:H_2O$ (=1:1:7) followed by a dip in a diluted HF solution (HF: H_2O=1:10) to remove the surface oxide. Substrates were then loaded directly into the growth chamber where the base pressure was 10^{-9} torr, and heated at 750°C to remove surface contamination.

An excimer laser using ArF was employed for the laser ablation of a CeO_2 target to deposit the CeO_2 film on Si. During deposition, the substrate was maintained at 500 °C to 750 °C and the pressure was maintained at 10^{-8} torr. After deposition, one part of the wafer was annealed *ex situ* in a furnace at 900 °C for 50 min. in a dry oxygen atmosphere.

X-ray diffraction and RHEED indicated the existence of single crystal CaF2-type CeO_2 deposited on the Si (111) substrate. The interface structure of the samples were investigated by high resolution electron microscopy (Topkon ATM 002B :HRTEM) using cross sectional thin foils. The HRTEM was operated at 200 KV with the spherical aberration of 0.4 mm. Auger electron spectroscopy (JEOL JAMP30: AES) was also employed to investigate depth profiles of the cerium, silicon, and oxygen elements in the samples. This analysis was carried out at the same sputtering rate and same probe current for both the as-grown and annealed samples. KLL transitions were selected for Si and oxygen, and the MNN transition was used for cerium to avoid signal overlapping in the spectra.

Figure 1 shows a HRTEM image of the interfacial structure of an as-deposited CeO_2 film grown at 750°C on a Si (111) surface. Between the CeO_2 overlayer and the Si (111) substrate

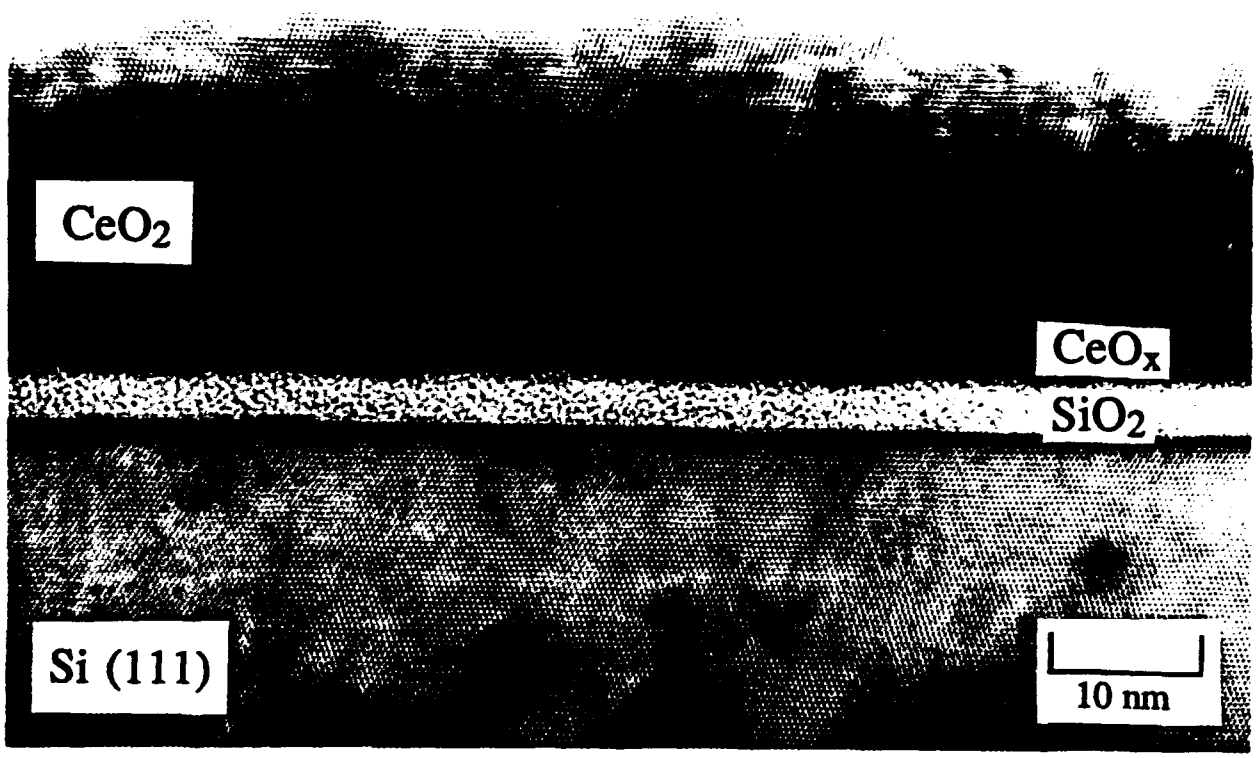

Figure 1. A lattice image of an as deposited sample from <110> direction. Single crystalline CeO_2, amorphous CeO_x (dark contrast region) followed by SiO_2 (bright contrast region) were observed on the Si (111) substrate. CeO_2 has a B-type orientation to the Si substrate.

there exist two distinct amorphous layers with dark and bright contrast respectively. The observed single crystal lattice image of the top layer corresponds to the CaF_2-type CeO_2. The CeO_2 has the B-type orientation, which is a twin with 180° rotation, to the Si (111) substrate [20]. The dark contrast in the crystalline CeO_2 region is thought to be a strain field. The thickness of the dark and bright amorphous regions in Fig. 1 are 6nm and 4nm respectively. The total thickness of the amorphous regions is 10 nm, which is too thick to be considered a native oxide. Figure 2 shows the interface structure as modified by post annealing at 900 °C for 50 min. in O_2 ambient. This figure indicates that the dark amorphous region has disappeared and the thickness of bright amorphous region increased. The CeO_2 layer still maintained the B-type orientation to the Si substrate.

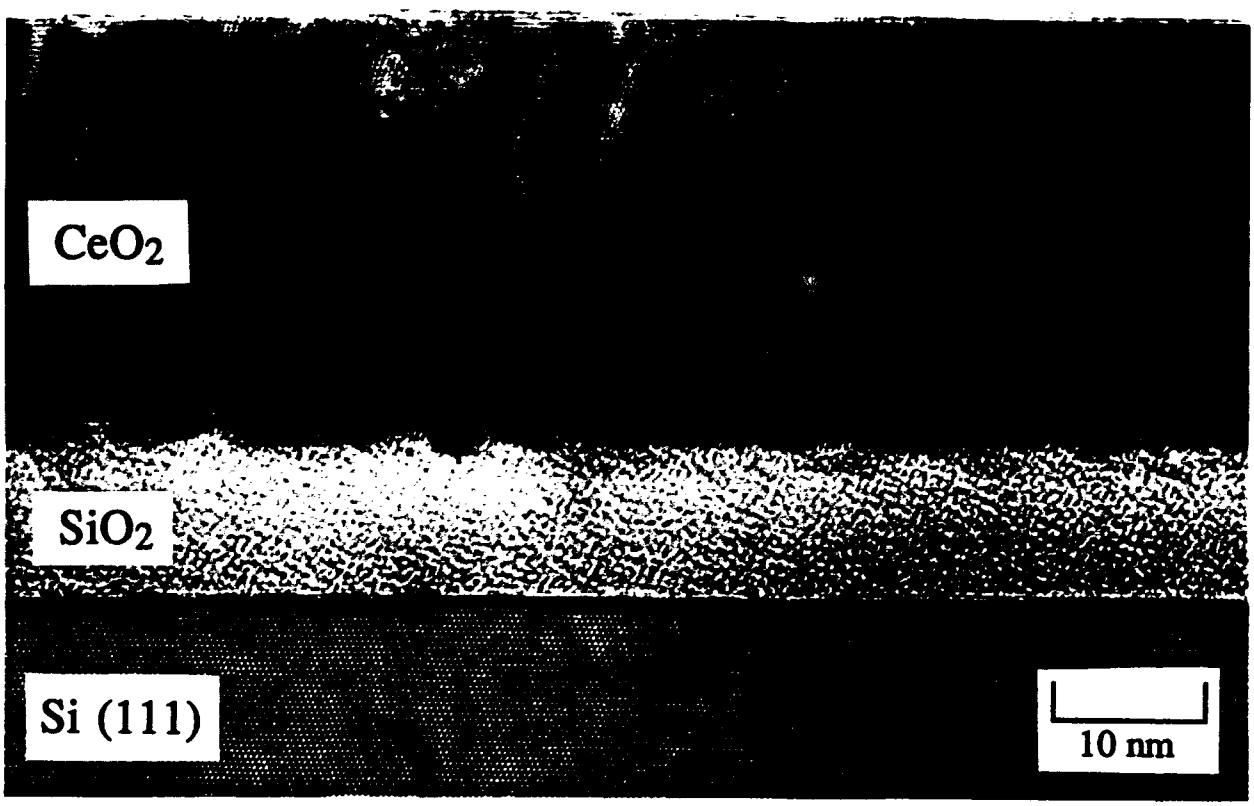

Figure 2. A lattice image of a sample after the post annealing in oxygen atmosphere observed from <110> direction. The dark amorphous region disappeared and the bright amorphous region grew, indicating the regrowth of CeO_2 and growth of SiO_2.

Figure 3 (a) shows a depth profile of Ce, Si, and oxygen in the as-deposited sample from AES analysis. In Figure 3 (a), from the surface to the interface, the cerium and oxygen profiles are constant. At the interface region between CeO_2 and Si substrate, the graded slope

of the oxygen profile can be seen. This indicates that a concentration gradient of oxygen exists in the interfacial region. In the post-annealed sample, as shown in Figure 3 (b), the cerium and oxygen profiles are also constant from the surface to the interface. However, the slope of the oxygen profile at the interface is sharply reduced, and is followed by a short plateau, indicating the existence of another phase. From this profile, it is speculated that the CeO_2 in the post-annealed sample has an abrupt interface in stoichiometry with the underlying SiO_2 phase.

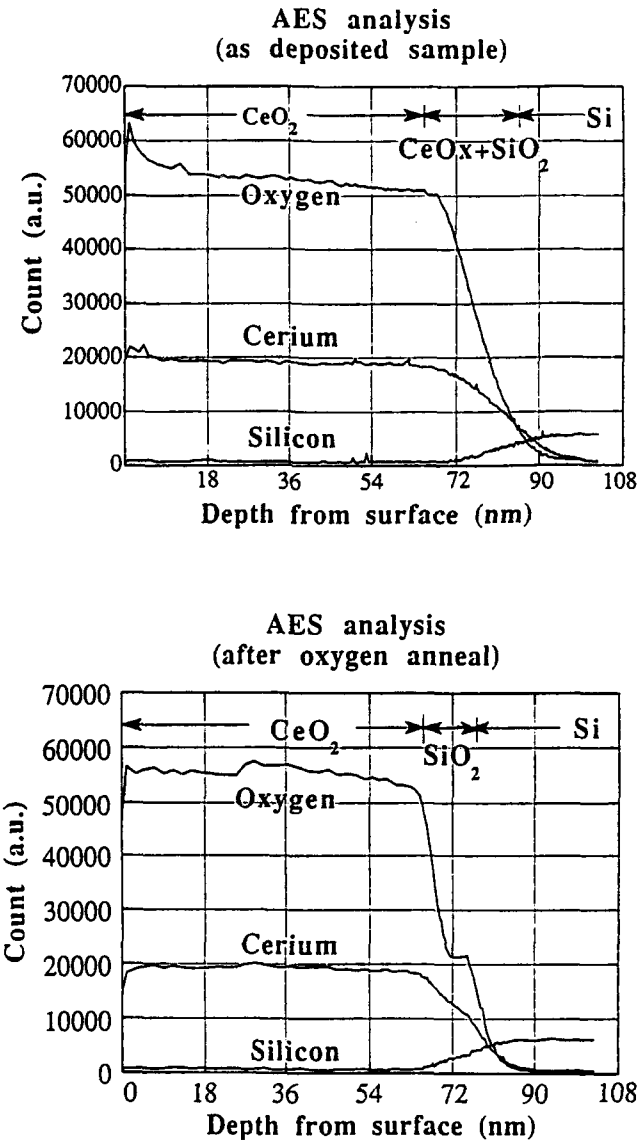

Figure 3. In-depth profile of Ce, Si and oxygen in as-deposited sample (a) and post-annealed sample (b). In as-deposited sample (a), gradual profile of oxygen at interface indicated the presence of oxygen deficient CeOx. In the post-annealed sample (b), a steep oxygen profile near interface means a sharp stoichiometric interface of CeO_2/SiO_2. The observed short flat profile of oxygen at the interface corresponds to the SiO_2 region.

As show in Figure 1, single crystalline CeO_2 was observed on the amorphous layers. The CeO_2 crystal seems to inherit a crystallographic information from the substrate because the B-type oriented CeO_2 single crystal is observed. From this, it is speculated that a reaction has occurred during the epitaxial growth of CeO_2 on Si substrate.

According to thermodynamic data [21], there is a possibility of a reaction expressed by:

$$4CeO_2+Si \rightarrow 2Ce_2O_3+SiO_2 \quad \Delta H_f = -46.4 \text{ Kcal/mole.} \tag{1}$$

where ΔH_f is the heat of formation for the reaction. During growth, oxygen atoms in the CeO_2 layer are released from their lattice sites, resulting in the formation of an oxygen deficient CeO_x region. It is possible that this oxygen deficient CeO_x layer corresponds to the dark amorphous layer in Figure 1. Oxygen atoms from the CeO_2 layer diffuse into the Si substrate, forming amorphous SiO_2. This SiO_2 layer should have bright contrast, as observed by HRTEM in Figure 1. The proposed oxygen deficiency at the interface coincides with the graded oxygen profile established by AES analysis at the interface in the as-deposited sample.

The oxidation at 900°C in oxygen atmosphere altered the structure to that of $CeO_2/SiO_2/Si$ (111). The recrystallization of amorphous CeO_x seems to occur from the CeO_2 layer to the underlying CeO_x layer by oxygen supplied during annealing Also, the SiO2 grew thicker due to oxygen diffusing to the Si substrate. At this CeO_2/SiO_2 interface, the stoichiometric change should be abrupt. The thicker SiO_2 region in the post-annealed sample is thought to be expressed as the short flat region in the oxygen profile shown in Figure 3 (b). The proposed reaction and recrystallizing process is schematically illustrated in Figure 4.

In summary, the interface structure of CeO_2/Si (111) was investigated by HRTEM and AES. At the CeO_2/Si interface, a reaction occurred forming an oxygen deficient, amorphous CeO_2 layer and SiO_2 layer. Annealing in oxygen atmosphere caused the recrystallization of CeO_2 and increased the thickness of the amorphous SiO_2 layer. This structure seems to have a great potential for the SOI device application, since the SiO_2/Si interface is expected to have a low density of interfacial states and a high breakdown voltage.

The authors would like to acknowledge Dr.H.Tsuya of the Research Center of NEC Co. for his fruitful discussions about SOI. Also the authors are grateful to Joan O'Sullivan for her help in their experiments. This work is supported by the Office of Naval Research.

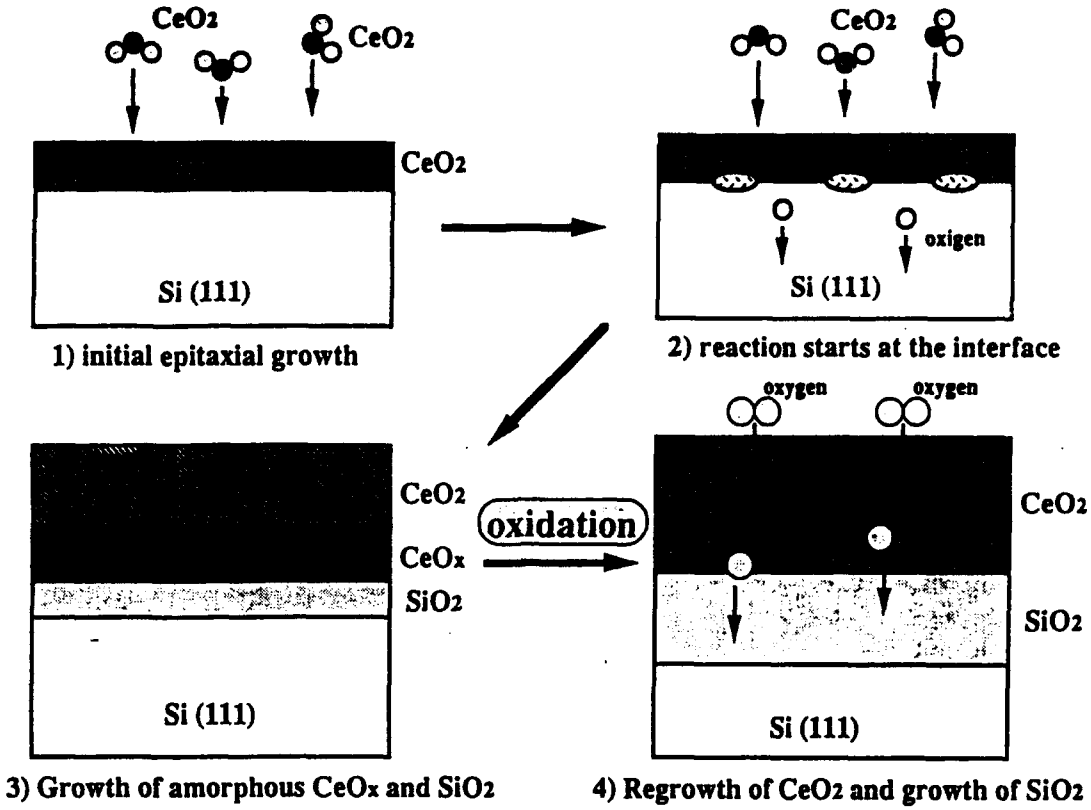

Figure 4. A schematic illustration of the interfacial reaction: 1) Initial stage of epitaxial CeO_2 growth, 2) During the growth of CeO_2, the reaction starts at the interface, 3) With further deposition, the sample has a $CeO_2/\alpha\text{-}CeO_x/\alpha\text{-}SiO_2/Si$ (111) structure and 4) After the annealing in oxygen ambient, the structure changes to $CeO_2/SiO_2/Si$ (111).

References

1. for example, T. Nishimura, Y. Akasaka and H. Nakata, in the *Silicon-on-Insulator: Its Technology and Application,* edited by S. Furukawa, (KTK Scientific Publisher, Tokyo, (1985) p. 263-268.
2. for example, J. C. Strum, Mat. Res. Soc. Symp. Proc. **107**, 295 (1988).
3. Y. Kunii, M. Tabe, and K. Kajiyama, J. Appl. Phys. **54**, 2847 (1983).
4. A. Ogura, and H. Terao J. Appl. Phys. **62**, 4170 (1987).
5. K. Izumi, M.Doken, and H. Ariyoshi, Electron. Letts. **14**, 593 (1978).
6. J. B. Lasky, Appl. Phys. Lett. **48**, 78 (1986)
7. M. Shimbo, K. Furukawa, K. Fukuda, and K. Tanizawa, J. Appl. Phys. **60**, 2987 (1986).
8. T. Ueno, T. Syowya, and I. Ohdomari, J. Appl. Phys. **69**, 808 (1991).
9. for example, S. J. Krause, C. O. Jung, T. S. Ravi, S. R. Wilson, and D. E. Burke, Mat. Res. Soc. Symp. Proc. **107**, 93 (1988).
10. K. Sugihara, S. Kusunoki, Y. Inoue, T. Nishimura, and Y. Akasaka, J. Appl. Phys. **62**, 4178 (1987)
11. H. Ishiwara and T.Asano, Appl. Phys. Lett. **40**, 66 (1982).
12. K. Egami, M. Mikami, and H. Tsyu, Appl. Phys. Lett. **43**, 757 (1983).
13. Y. Hokari, M. Mikami, K. Egami, and H. Tsuya, IEEE J. Solid-State Circuit **SC-20**, 173 (1985).
14. D. K. Fork, F. A. Ponce, J. C. Tramontana, and T. H. Geballe, Appl. Phys. Lett. **58**, 2294 (1991)

15. T. Asano and H. Ishiwara, J. Appl. Phys. **55**, 3566 (1984).
16. M. Sasaki, H. Onda, and N. Hirashita, Mat. Res. Soc. Symp. Proc. **53**, 149 (1986).
17. T. Inoue, Y. Yamamoto, S. Koyama, and S. Suzuki, Appl. Phys. Lett. **56**, 1332 (1990).
18. M. Yoshimoto, H. Nagata, T. Tsukahara, and H. Koinuma, Jpn. J. Appl. Phys. **29**, L1199 (1990)
19. T. Inoue, M. Osonoe, H. Tohda, and M. Hiramatsu, J. Appl. Phys. **69**, 8313 (1991).
20. R. T. Tung, J. M. Gibson, and J. M. Poate, Appl. Phys. Lett. **42**, 888 (1083).
21. in the *Metallurgical Thermochemistry* edited by O. Kubaschewski and C. B. Alcock (Pergamon, New York, 1979) p. 278.

VI. Distribution List

Mr. Max Yoder Office of Naval Research Electronics Division, Code: 314 Ballston Tower One 800 N. Quincy Street Arlington, VA 22217-5660	3
Administrative Contracting Officer Office of Naval Research Resident Representative The Ohio State University Research Center 1960 Kenny Road Columbus, OH 43210-1063	1
Director, Naval Research Laboratory ATTN: Code 2627 Washington, DC 20375	1
Defense Technical Information Center Bldg. 5, Cameron Station Alexandria, VA 22314	2